Collective cell guidance by cooperative intercellular forces.

Dhananjay T. Tambe[1]*, C. Corey Hardin[2]*, Thomas E. Angelini[3], Kavitha Rajendran[1], Chan Young

Park[1], Xavier Serra-Picamal[4], Enhua Zhou[1], Muhammad Zaman[5], James P. Butler[1], David A. Weitz[3],

Jeffrey J. Fredberg[1], Xavier Trepat[4]

* contributed equally

[1]Program in Molecular and Integrative Physiological Sciences, School of Public Health, Harvard University,
Boston MA, 02115, USA.
[2]Division of Pulmonary and Critical Care Medicine, Massachusetts General Hospital, Boston MA, 02114, USA.
[3]School of Engineering and Applied Sciences, Harvard University, Cambridge, MA 02138, USA.
[4]Institut de Bioenginyeria de Catalunya, Universitat de Barcelona, and Ciber Enfermedades Respiratorias, 08036
Spain.
[5]Department of Biomedical Engineering, Boston University, Boston, MA 02215, USA

Cells comprising a tissue migrate as part of a collective. In order to coordinate collective multi-cellular migration, each constituent cell integrates local information including chemical signals and mechanical stresses.[1,2] The boundary between a constituent cell and its immediate neighbors comprises cell-cell junctions and cryptic lamellipodia[7], but the state of local mechanical stress exerted at that boundary has not been accessible experimentally. As such it is not clear how collective mechanical processes could be coordinated over length scales spanning large multi-cellular assemblies. We report here maps of the stresses exerted within and between cells comprising a monolayer. Within the cell sheet there arise unanticipated fluctuations of mechanical stress that are severe, emerge spontaneously, and ripple across the monolayer. These fluctuations define a rugged stress landscape that becomes increasingly heterogeneous, sluggish, and cooperative with increasing system density. Within that persistently rugged stress landscape, local cellular migrations are found to migrate along local orientations of maximal principal stress. Migrations of both endothelial and epithelial monolayers conform to this behavior, as do breast cancer cell lines before but not after the epithelial-mesenchymal transition. In these diverse cell types, our data indicate that collective migration is governed by a simple but unifying physiological principle: neighboring cells join forces to transmit appreciable intercellular normal stress across local cell-cell junctions, but migrate along orientations of minimal intercellular shear stress.

A variety of fundamental processes in development, health, and disease depend upon the

coordinated motion of cell groups [3]. To describe coordinated cellular motions in these processes, high-

throughput genomic approaches have identified molecular players and mapped their interaction into comprehensive signaling networks [4]. But even with detailed signaling and structural information in hand, the role of intercellular adhesion in collective migration is disputed [5], and our understanding of collective cellular migration lacks predictive power and remains largely descriptive. Central to these limitations is the absence of a physical picture that links cell motion to mechanical stresses exerted within the cell body and at cell-cell boundaries; these stresses have never been measured. Here we report high resolution maps of these stress components everywhere within an advancing monolayer sheet, which serves as a simple experimental model system. These stress maps reveal that the local cellular trajectory follows local stress fields that are severely heterogeneous and dramatically cooperative over distances spanning many cell bodies. Together, these findings reveal an unanticipated but unifying physiological principle, namely, that each cell tends to migrate and remodel so as to maintain minimal local intercellular shear stress. Detailed knowledge of the biology of the cell-cell junction, the cryptic lamellipodium, or any specific molecular event could never predict such a unifying principle because it is an emergent property of a multicellular collective system. By analogy to the well known guidance mechanisms of chemotaxis, durotaxis and haptotaxis, we call this distinct but innately collective mechanism plithotaxis, from the Greek "plithos" denoting crowd, swarm, multitude, or throng.

To measure the local state of stress within a monolayer (Fig. 1), we developed Monolayer Stress Microscopy, MSM (online supplement 1). On an inverted optical microscope, we record cell-generated displacements of fluorescent markers embedded near the surface of a collagen-coated polyacrylamide gel substrate on which the cells are adherent. From those displacements we then compute a map of the tractions forces, T, exerted by the monolayer upon the gel.[6] Finally, from these traction forces measured directly at the interface between the cell and its substrate, a straightforward balance of forces as demanded by Newton's laws is then used to obtain the distribution of the mechanical stress everywhere within the cell sheet (Fig. 1 a). Gradients of these stresses within the

2

cell sheet arise from the pileup of traction forces applied on the underside of the cells. Measured stresses within the monolayer sheet (Fig. 1 b) correspond to mean values over the full thickness (height, h) of the cell layer. At each point within the sheet the local coordinate system (Fig. 1 c) can be rotated in the cell plane in order to find those special orientations along which the local normal stress is maximal and minimal, respectively, thus defining the two principal stress components (σ_{max} and σ_{min}) and the two corresponding, mutually perpendicular, principal orientations (Fig. 1 d; Online Supplement 1). As such, the associated MSM result displays at high resolution, and maps separately, each individual component of the in-plane stress tensor.

We consider first the average local normal stress, simply defined as $\overline{\sigma} = (\sigma_{max} + \sigma_{min})/2$, and its spatial heterogeneity. A traditional image of an advancing monolayer of rat pulmonary vascular endothelial (RPME) cells is unremarkable (Fig. 2 a). The underlying distribution of local normal stress, by contrast, is severely heterogeneous; normal stresses were found to be mostly positive (tensile) with values exceeding 300 Pa in regions spanning tens of cells. These regions of predominantly tensile stresses alternate with regions of weakly negative (compressive) stresses (Fig. 2 b). These fluctuations occur steadily over distances spanning multiple cell widths and define a stress landscape that is rugged (Figs. 2b, k), by which we mean that the spatial fluctuations over these relatively short distances are comparable in magnitude to the spatial mean values. We consider next the distribution of the intercellular shear stress (Fig. S1) which is not to be confused with any additional shear stress that might be imposed by flow on the monolayer surface, which in this case is everywhere zero. As in the case of the normal stress, the shear stress at a point within a material varies with orientation and attains its maximal value, $\mu = (\sigma_{max} - \sigma_{min})/2$, at 45$^\text{o}$ from the principal orientations (Fig. 1 d). The local maximal shear stress was systematically smaller than the local normal stress, but was also characterized by a rugged landscape (Fig. 2 c). As the monolayer advances, these respective stress landscapes evolve continuously in time (supplemental movie SM1).

3

Finally, dependence of local stresses upon orientation signifies stress anisotropy. To visualize this anisotropy, we plotted ellipses whose major axis corresponds to the local σ_{max} and minor axis corresponds to the local σ_{min}, each aligned with corresponding principal orientations. Where $\sigma_{max} = \sigma_{min}$ the stress field is isotropic, the ellipse becomes a circle, μ is zero, and there exists no preferred stress orientation. But where $\sigma_{max} >> \sigma_{min}$ the local stress field is highly anisotropic, the ellipse becomes spindle-like, μ is nonzero, and there exists a strongly preferred and well-defined stress orientation. From region-to-region, we found that ellipse size, ellipse shape, and ellipse orientation varied extensively, but with strong local correlations (Fig. 2 e).

As cells extend cryptic lamellipodia[7] and advance within the monolayer stresses at every point and at every instant of time must be in mechanical balance. Nonetheless, no mechanistic framework or physical picture yet exists that might link these stresses to cellular orientation, remodeling, or migration. In the case of the single cell in isolation, by contrast, uniaxial stretch can cause the cell to reorient to some defined angle relative to the applied stress, from parallel to perpendicular, depending upon the time scale of the mechanical perturbation. Here we ask in the case of the monolayer, to what extent are intercellular stresses are meaningful biologically and useful predictively? The answer to this question is suggested by two pieces of experimental evidence. First, since phase-contrast images and stress maps are mutually independent measurements, the coincidence between orientation of the cell body versus orientation of the maximal principal stress is striking (Fig. 2 e). Further, because the maximal principal orientation corresponds to the local axis of highest normal stresses and zero shear stress, this result suggests that the cell-cell junction, as well as the cell body, support high normal stresses, which are overwhelmingly tensile, but only minimal shear stresses. One would predict, therefore, that local stress fibers might align with maximal principal orientations, and for the spindle-like RPME cells this is in fact seen to be the case (Fig. 2 e). Second, cells not only align with the maximal principal orientation, but also migrate along that orientation (Fig. 2 e, red arrows;

supplemental movie SM2). Appreciable portions of the stress field are approximately isotropic, however, and therefore the local orientation of cell motion would not be expected to correlate with a stress field possessing no preferred orientation.

As such, these observations lead naturally to the following prediction: regions of higher stress anisotropy will exhibit stronger alignment between the direction of local maximal principal stress and that of local cellular migration velocity. To test this prediction, we reasoned as follows. Since the maximum local shear stress is given by $\mu = (\sigma_{max} - \sigma_{min})/2$, we took μ as a direct and quantitative index of stress anisotropy. We then rank-ordered this stress anisotropy by quintiles. For each point within the cellular monolayer falling within any given quintile, we measured the alignment angle ϕ between the orientation of the local maximal principal stress and the orientation of the local cellular migration velocity vector (Fig. 2 f, inset). The greater was the local shear stress, the narrower was the distribution of ϕ (Fig. 2 f, g, h). We then constructed the cumulative probability distribution function, $\overline{P}(\phi)$, reasoning that if there were perfect alignment between the orientation of local cellular migration velocity and that of local maximal principal stress, then all angles ϕ would be $0°$ and the cumulative probability distribution would be a step function from probability 0 to probability 1 occurring at $0°$. If there were no alignment, however, then all angles between $0°$ and $90°$ would be equally likely, and the cumulative probability function would be a straight line from probability 0 at 0° to probability 1 at $90°$. In the regions with lowest stress anisotropy (blue), the angular distribution was broad but not uniform. In regions with highest stress anisotropy (red), the angular distribution was quite narrow; the orientation of cellular velocity and the orientation of maximal principal stress were coupled strongly. The stronger the stress anisotropy the greater the overall degree of alignment.

To assess the generality of this finding, we then examined monolayers comprising Madin-Darby canine kidney (MDCK) cells (Fig. 2 j), which were of particular interest because they are epithelial, not endothelial, and because they are rounded in the plane, not spindle-shaped as are RPME

5

cells. Despite these differences in cell type and cell morphology, the stresses were heterogeneous (Fig. 2 k, l) and the local orientation of cellular migration was also found to follow the local orientation of maximal principal stress (Fig. 2 m, n). To assess further the generality of this finding, we next examined the behavior of monolayers of well-established breast-cancer model systems: MCF10A cells (control or vector) (Fig. 3 a), MCF10A cells overexpressing ErbB2/HER-2/neu (Fig. 3 b), and MCF10A cells overexpressing 14-3-3ζ (Fig. 3 c). We chose these cell lines because each exhibits pronounced morphological differences as well as diverse levels of transforming potential, expression of cell-cell junction proteins, and cell proliferation.[8] For these three monolayers systems the traction forces were comparable in magnitude (Fig. 3 d, e, f) but, compared with control cells (Fig. 3 g) and ErbB2 cells (Fig. 3 h), the normal intercellular stresses in the 14-3-3ζ cell sheets (Fig. 3 i) were substantially smaller. Because 14-3-3ζ cells have decreased expression of cell-cell junctional markers[8], this finding is also consistent with limited transfer of physical forces from cell-to-cell. Much as in the case of endothelial cells and control epithelial cells, ErbB2 cells moved in alignment with the direction of maximum principal stress. By contrast 14-3-3ζ cells, which have poor cell-cell contacts, were seen to move nearly independently of the orientation of the maximum principal stress (Fig. 3 m). To assess further the importance of cell-cell adhesion, we weakened cell-cell contacts of MCF10A vector cells by calcium chelation. As expected, weakening of cell-cell junctions (Fig. 4 g, i) caused prompt ablation of the rugged stress landscape (Fig. 4 h, j), and simultaneously weakened coordination between local stress orientations and local cellular motions (Fig. 4 s, magenta). Both the ruggedness of the stress landscape and the guidance of motion by stress recovered upon returning to normal growth medium (Fig. 4 i, s, blue), but this reversibility was blocked in the presence of E-cadherin antibodies (Fig. 4 r, s, red). Together, these observations establish that transmission of stresses across many cells is necessary for the cells to follow the local orientation of the maximal principal stress.

For collective migration to be coordinated across many cells, intercellular stresses might be expected to be cooperative over comparable distances. To quantify the spatial extent of any such stress cooperativity, we first examined the spatial autocorrelation function of the average normal stress:

$$C(R) = \frac{1}{N \operatorname{var}(\overline{\sigma})^2} \sum_{i,j=1 | \vec{r}_i - \vec{r}_j | = R}^{N} \delta \overline{\sigma}_i \cdot \delta \overline{\sigma}_j$$

where $\delta \overline{\sigma}_i$ is the local departure of the average normal stress at position $\vec{r}_i$ from its spatial mean $< \overline{\sigma}_i >$, $\operatorname{var}(\overline{\sigma})$ is the variance of those departures, and the notation $\left| \vec{r}_i - \vec{r}_j \right| = R$ means equality within a uniform bin width of 5 microns. Confining attention to regions many cell lengths from the leading edge of an MDCK monolayer (Fig. 5 a), fluctuations in normal stress (Fig. 5 c) were found to be correlated over a length scale of approximately 10-15 cell diameters (Fig. 5 e, blue). Cooperativity of normal stresses over 10-15 cell diameters can be attributable to alignment of principal stresses end-to-end, as in a tug-of war, or side-by-side, as police who lock arms during crowd control. To assess whether normal stresses are aligned according to either of these configurations, we decomposed the maximum principal stress into end-to-end and side-by-side contributions,

$$C_{end}(R) = \frac{1}{N \|F\|^2} \sum_{i,j=1 | \vec{r}_i - \vec{r}_j | = R}^{N} \vec{F}_i \cdot \vec{F}_j \cos^2 \theta_{ij} \qquad C_{side}(R) = \frac{1}{N \|F\|^2} \sum_{i,j=1 | \vec{r}_i - \vec{r}_j | = R}^{N} \vec{F}_i \cdot \vec{F}_j \sin^2 \theta_{ij}$$

where $\|...\|$ denotes L^2 norm, F_i is the local maximal principal stress considered as a vector quantity (such that the angle between the maximal and minimal principle stress orientations is taken modulo π) and θ_{ij} is the angle between adjacent vector pairs. The two components were found to contribute almost equally to force cooperativity, thus indicating the coexistence of both end-to-end and side-by-side force correlations (Fig. 5 f). Simply put, in order to move cooperatively neighboring cells join forces.

Cooperative motions emerge naturally in inert particulate systems that exhibit close-packing, structural disorder, and glassy dynamics, such as colloidal glasses [9]. A central feature that identifies

7

these systems as being glassy is the slowing of internal structural rearrangement as system density is increased; with increasing system density, each particle becomes increasingly trapped by its neighbors so that, in order to rearrange at all, many neighboring particles must rearrange cooperatively [10]. As such, the size of cooperative clusters increases as system density increases. Moreover, as size of the cluster grows the number of possible structural rearrangements decreases and, as such, the time needed for cooperative rearrangements increases precipitously until, eventually, the system becomes virtually frozen, or stuck [10]. Might the monolayer cell sheet exhibit such signatures of glassy dynamics? To answer this question we analyzed motion of the MDCK monolayers as cellular density increased with the passage of time [1,6]. Consistent with an expectation of glassy dynamics, the spatial decay in $C(r)$ was smaller when the density was greater (Fig. 5 e, red curve with corresponding monolayer and force map Fig. 5 b, d), indicating that force cooperativity extended to greater distances. As a direct measure of slowing of structural rearrangements we turned to metrics commonly used in soft condensed matter systems. We consider the average number of cells which change position between two points in time, which defines an overlap function q_s:

$$q_s = \frac{1}{N} \sum_1^N w(|\vec{r}_i(t) - \vec{r}_i(t=0)|)$$

where the weight function w is equal to 1 if the distance between cell positions at sequential times is less than half a cell diameter, and zero otherwise. The variance of q_s is then a measure of the rate of overall structural rearrangement and is related to the so-called four-point susceptibility χ^{ss} [11]. The peak in χ^{ss} occurs at the overall structural relaxation time, and the height of that peak is related to the size of rearranging regions [12]. If the system is glassy, the peak in χ^{ss} is expected to shift towards longer times as system density is increased, and a clear shift of the peak in the more dense system confirms this expectation (Fig. 5 g). The peak height also increases in the more dense system, confirming the presence of growing velocity clusters. Moreover, these density-dependent shifts in the

8

position and the peak height of χ^{ss}, which are indicative of slowing of structural rearrangements, occur simultaneously with growth of force clusters as indicated by the slowing decay in the force autocorrelation function with increasing density (Fig. 5 e, red). Although a mechanistic link between inter-particle forces and spatially heterogeneous dynamics in glassy systems remains unclear [13], the findings of Fig. 5 are consistent with approach to a glass transition.

Recent advances have unraveled important features of stress transmission across specific molecular constituents of the focal adhesion and of the adherens junction, including vinculin, talin, and α-catenin for example [14], but the integrative context of these molecular events within integrated stress-bearing structures comprising highly redundant molecular pathways, or even across multi-cellular assemblies at larger scales of organization, have remained largely ambiguous. Logically, associated integrative principles have remained unstudied. Because distinct stress tensor components between contiguous cells in any complex living system have never before been measured, Monolayer Stress Microscopy now sets the study of underlying molecular events within an integrative mechanical context that is conceptually comprehensive and experimentally rigorous. The finding that each cell comprising a monolayer tends to migrate and remodel so as to maintain minimal local intercellular shear stress complements other integrative physiological principles (Online supplement 3).

A central question in morphogenesis and disease is how differentiated structures emerge from homogeneous cell populations [15]. Differentiation and pattern formation in multi-cellular systems is currently explained by the existence of morphogenetic gradients and by local variations in the composition, topology, and stiffness of the extracellular matrix [16]. In addition, once transduced by the sensory machinery of the individual cell [17], the spontaneously emergent rugged stress landscape reported here would be expected to trigger non-uniform secretion of soluble or insoluble factors, thus altering the local cellular microenviroment, causing cytoskeletal reinforcement [18] or cytoskeletal fluidization [19], as well as activating in a highly non-uniform fashion stress-dependent genetic programs

that give rise to differentiated tissues. These emergent stress heterogeneities are severe and persistent

but unanticipated. How they might become harnessed and regulated during morphogenesis or repair

and, perhaps more importantly, how they might become unharnessed or dysregulated during disease or

injury, we identify here as major open questions, but ones that are now accessible to direct

experimental attack.

Figure 1 | Monolayer stress microscopy. (**a**) Simplified representation of physical relationship between cell-substrate tractions, T, which have been reported previously[6], and intercellular stresses, σ, which are reported for the first time here. The intercellular stresses are generated from transfer of local as well as distant unbalanced cell-substrate tractions. At any point within the monolayer (**b**), the intercellular stresses, defined in laboratory frame (x, y), (**c**), have shear (σ_{xy}, and σ_{yx}) and normal (σ_{xx}, and σ_{yy}) components. This frame can be rotated locally to obtain the principal frame (x', y'), (**d**), where shear stresses vanish and the resulting normal stresses are called principal stresses (σ_{max} and σ_{min}). The corresponding axes are called maximum, aligned with x', and minimum, aligned with y', principal orientations.
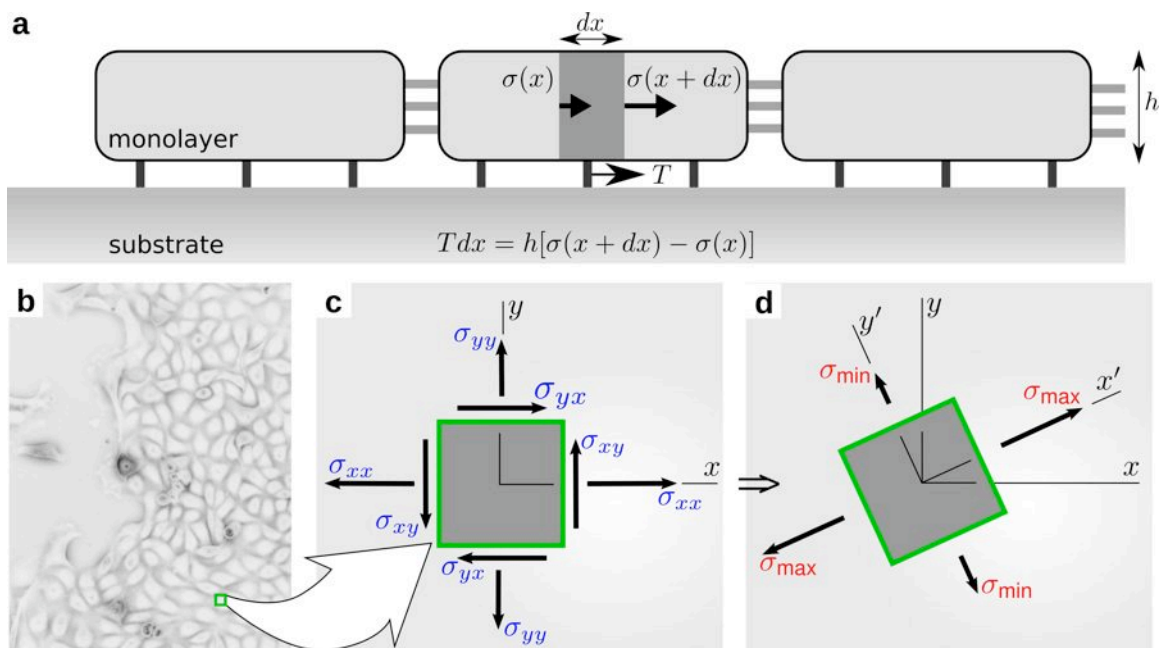
Figure 2 | Intercellular stress maps and mechanical guidance of collectively migrating monolayers. (**a**) Transmitted light image of rat pulmonary microvascular endothelial (RPME) cell monolayer. Corresponding to this image are the maps of average normal stress (**b**), which is predominately tensile but forms a rugged stress landscape (**c**), the maximum shear stress (**d**), principal stress ellipses (blue) and cell velocity vectors (red) (**e**). The alignment angle, ϕ, between major axis of the principal stress ellipse and direction of the cellular motion (**f, inset**) shows that the greater the local shear stress the narrower is the distribution of ϕ (**f, g, h**). The cumulative probability distribution $\overline{P}(\phi)$ varied strongly and systematically with stress anisotropy (**i**); curves from blue, to red are in the order of higher quintiles. Comparable maps are found for the Madin-Darby canine kidney (MDCK) monolayer (**j-n**). Note that the average tensile stress (**k**) increased systematically with increasing distance from the advancing front thus contributing to the state of global tug-of-war [6]. Vertical size of the images of monolayer: RPMEC - 545 μm, MDCK - 410 μm. Each curve in (**i**) and (**n**) and distributions in (**f**), (**g**), and (**h**) have more than 8,000 observations.
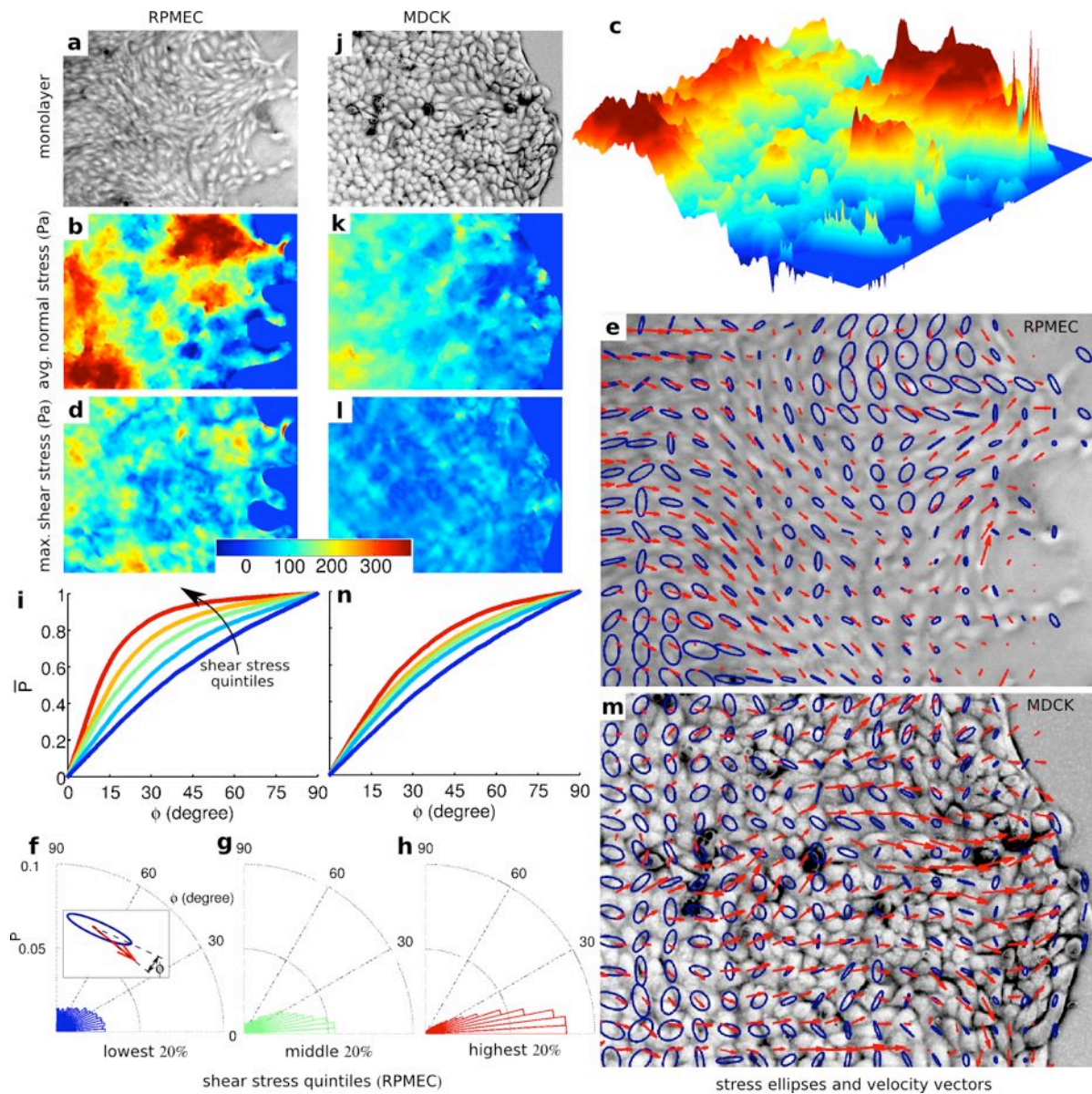
Figure 3 | Systematic changes in the stress maps and force motion relationship. Phase contrast image of nontransformed human mammary epithelial cell line, MCF10A, control or vector (**a**), cells overexpressing ErbB2 (**b**), and 14-3-3ζ (**c**). Maps of cell-substrate tractions, T_x, (**d, e, f**), normal stress (**g, h, i**), and maximum shear stress (**j, k, l**) corresponding to each of these three mammary epithelial cell lines. (**m**) Cumulative probability distribution of ϕ for the regions corresponding to highest quintile of the shear stress for five different cell sheets. Vertical size of the images of monolayer: 410 μm. Each curve in (**m**) has more than 8,000 observations.
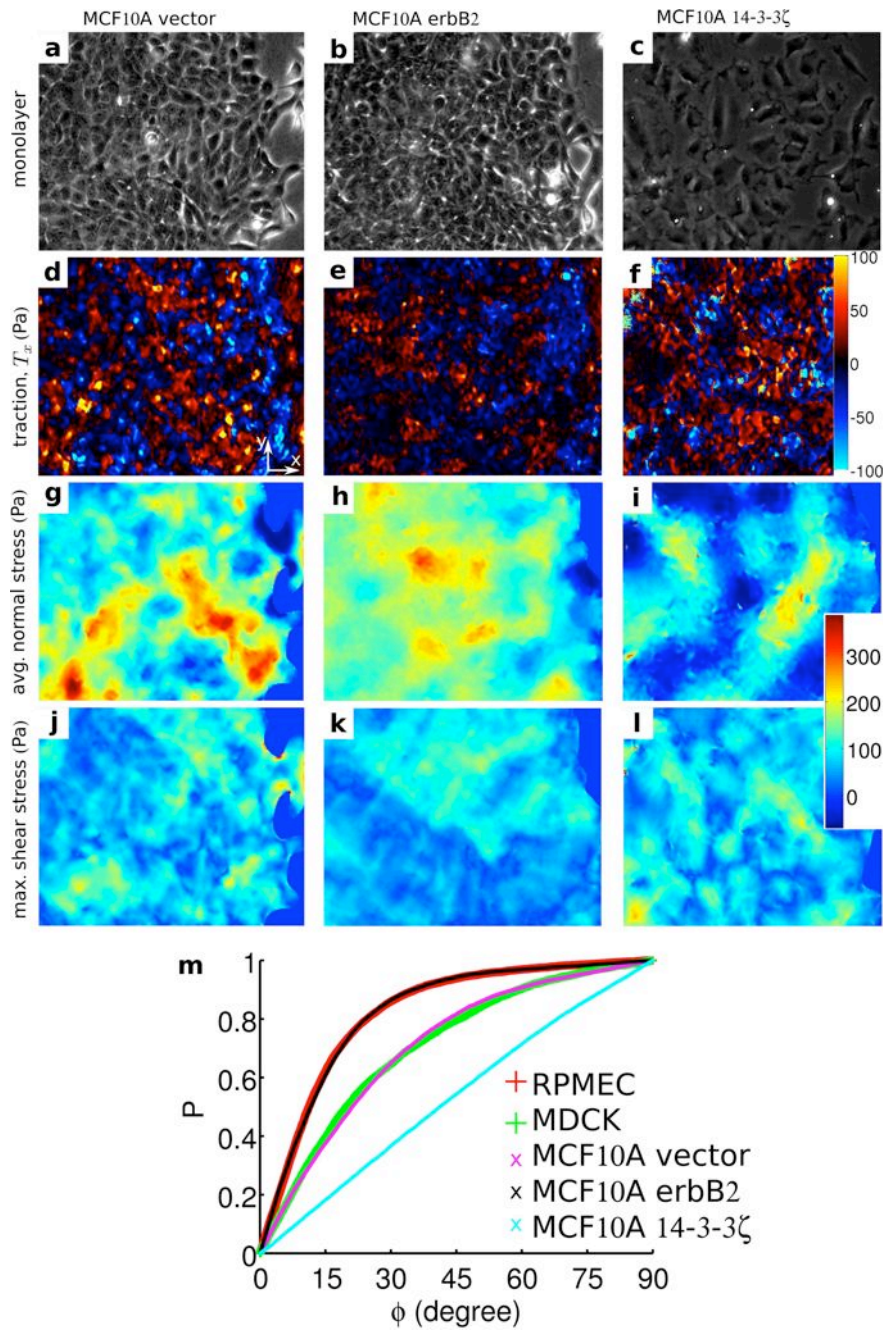
Figure 4 | Local cell guidance requires long-range force transmission. Time-controls of intercellular stress maps of MCF10A-vector cell monolayers (**a-f**). The stress patterns do not change appreciably over a period of 80 minutes. After 10 minutes in presence of the calcium chelator EGTA (4mM), however, cells lose contacts with their neighbors (**g**, **i** and **m**, **o**). These changes lead to attenuation of intercellular average normal stress (**h**, **j** and **n**, **p**). After returning to normal growth medium for 80 minutes, the stresses and the cell-cell contacts are largely restored (**k**, **l**), but if the growth medium is supplemented with E-cadherin antibody (7 μg/ml) recovery of stresses and cell-cell contact is blocked (**q, r**). EGTA treatment widens the distribution of angle (ϕ) between local cellular velocity and local maximum principal orientation (**s**). The distribution of ϕ is narrowed if calcium is restored (**s**, blue curve), but widened further if the restoration medium is supplemented with E-cadherin antibody (**s**, red curve). Together, these data show that local cell guidance requires long-range force transmission across cell-cell junctions. Increased intensity at cell boundaries in phase contrast images (panels **i**, **o**, and **q**) reveals disruption of cell-cell junctions. Vertical size of the images of monlayer: 410 μm. Each curve in (**s**) has more than 1,500 observations.
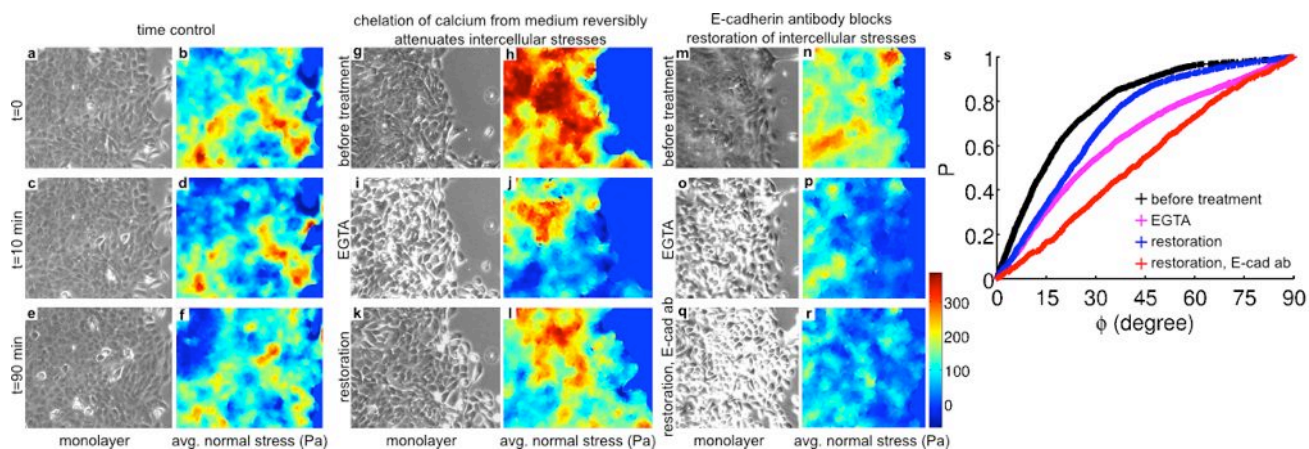
Figure 5 | Signatures of cooperativity and associated glassy dynamics. Phase contrast images of a monolayer of Madin-Darby canine kidney (MDCK) cells well away from the leading edge at early (**a**, t=196 min, density=1681±88 cells/mm^2) and late (**b** , t=3196 minutes, density=2487±218 cells/mm^2) times. Also shown are corresponding maps of average normal stress (**c, d**). Note that any contribution to the stress field with a wavelength longer than the size of the field of view is not included in the calculation. Thus a stress build up extending over the entire monolayer as previously reported [6] is absent from this analysis. (**e**) Time averaged spatial autocorrelation function, $C(r)$, of average normal stress in low density (1681 cells/mm^2, blue), and high density (2487 cells/mm^2, red) regions. (**f**) $C(r)$ of high density maximal principal stress resolved into components representing force chains (circles) and force clusters (squares). (**g**) Variance, χ^{ss}, of the self-overlap parameter, q_s, as a function of time, in early, low denisty (t=1-270 minutes, 1699 ±40 cells/mm^2, blue) and late, high density (t= 1800-2070 minutes, 1950±156 cells/mm^2, red) intervals. Each curve represents an average over three successive 90 minute windows of similar density. Error bars represent the standard deviation over the square root of the number of windows. Vertical size of the images of monolayer: 480 μm.

15
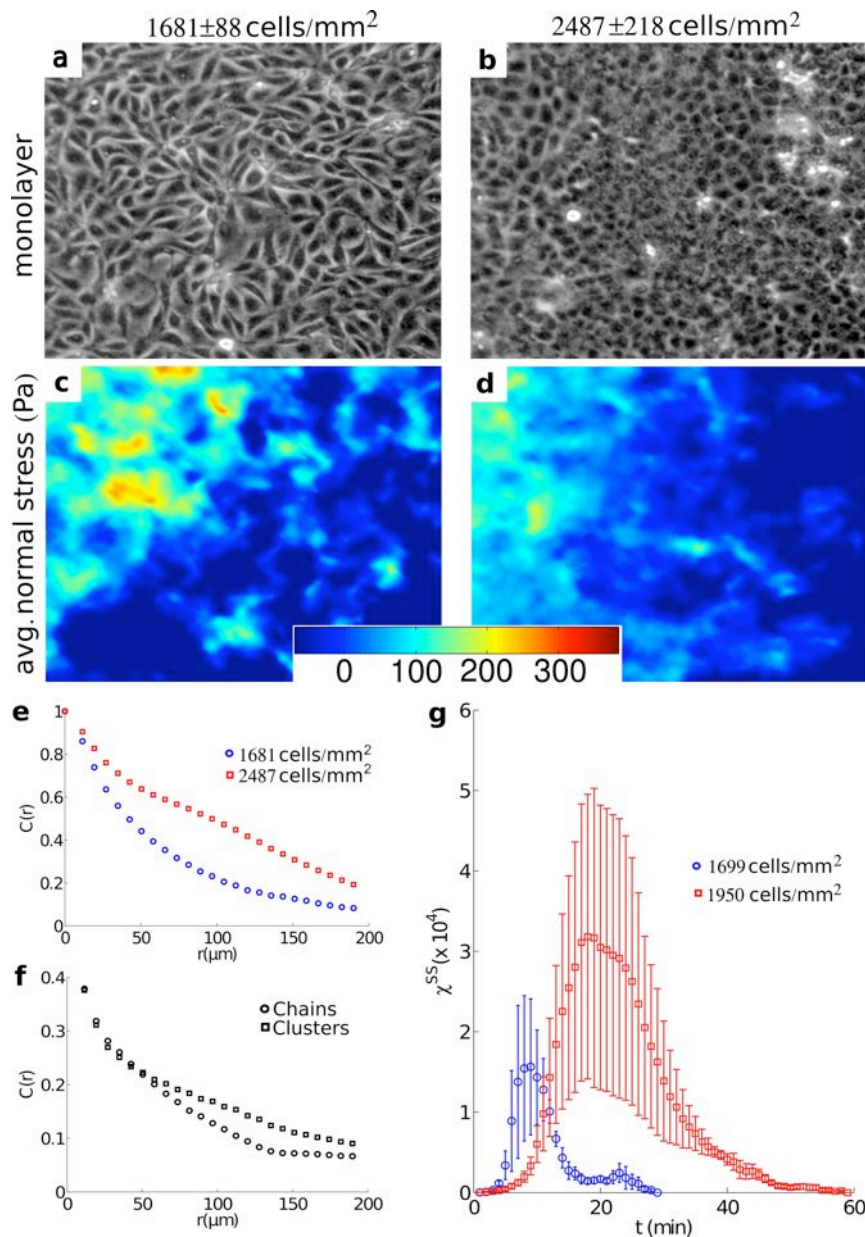
List of References

1   **Thomas E. Angelini, Edouard Hannezo, Xavier Trepat et al., *Physical Review Letters* 104 (16), 168104 (2010).**

2   **D. T. Butcher, T. Alliston, and V. M. Weaver, *Nature reviews* 9 (2), 108 (2009); D. Discher, C. Dong, J. J. Fredberg et al., *Ann Biomed Eng* 37 (5), 847 (2009); S. Kumar and V. M. Weaver, *Cancer Metastasis Rev* 28 (1-2), 113 (2009); K. R. Levental, H. Yu, L. Kass et al., *Cell* 139 (5), 891 (2009); M. J. Paszek and V. M. Weaver, *Journal of mammary gland biology and neoplasia* 9 (4), 325 (2004).**

3   **Ambra Bianco, Minna Poukkula, Adam Cliffe et al., *Nature* 448 (7151), 362 (2007); P. Friedl and D. Gilmour, *Nat Rev Mol Cell Biol* 10 (7), 445 (2009); Silvia Giampieri, Cerys Manning, Steven Hooper et al., *Nat Cell Biol* 11 (11), 1287 (2009); DJ Montell, *Science* 322, 1502 (2008); Tanya J. Shaw and Paul Martin, *Journal of Cell Science* 122 (18), 3209 (2009).**

4   **Kaylene J. Simpson, Laura M. Selfors, James Bui et al., *Nat Cell Biol* 10 (9), 1027 (2008); Philip Vitorino and Tobias Meyer, *Genes and Development* 22 (23), 3268 (2008).**

5   **M. Bindschadler and J. L. McGrath, *J Cell Sci* 120 (Pt 5), 876 (2007).**

6   **X Trepat, MR Wasserman, TE Angelini et al., *Nature Physics* 5, 426 (2009).**

7   **R. Farooqui and G. Fenteany, *J Cell Sci* 118 (Pt 1), 51 (2005).**

8   **Jing Lu, Patricia S. Steeg, Janet E. Price et al., *Cancer Research* 69 (12), 4951 (2009); Senthil K. Muthuswamy, Dongmei Li, Sophie Lelievre et al., *Nat Cell Biol* 3 (9), 785 (2001).**

9   **Giorgio Parisi and Francesco Zamponi, *Reviews of Modern Physics* 82 (1), 789 (2010).**

10   **E. R. Weeks, J. C. Crocker, A. C. Levitt et al., *Science* 287 (5453), 627 (2000).**

11   **L. Berthier, G. Biroli, J. P. Bouchaud et al., *Science* 310 (5755), 1797 (2005).**

12   **AS Keys, AR Abate, S.C. Glotzer et al., *Nature Physics* 3, 260 (2007); Cristina Toninelli, Matthieu Wyart, Ludovic Berthier et al., *Physical Review E* 71 (4), 041505 (2005).**

13   **Randall W. Hall and Peter G. Wolynes, *The Journal of Physical Chemistry B* 112 (2), 301 (2007); Daniel M. Mueth, Heinrich M. Jaeger, and Sidney R. Nagel, *Physical Review E* 57 (3), 3164 (1998); V. Trappe, V. Prasad, Luca Cipelletti et al., *Nature* 411 (6839), 772 (2001).**

14   **Armando del Rio, Raul Perez-Jimenez, Ruchuan Liu et al., *Science* 323 (5914), 638 (2009); Carsten Grashoff, Brenton D. Hoffman, Michael D. Brenner et al., *Nature* 466 (7303), 263 (2010); K. Hu, L. Ji, K. T. Applegate et al., *Science* 315 (5808), 111 (2007); Quint le Duc, Quanming Shi, Iris Blonk et al., *J Cell Biol* 189 (7), 1107 (2010); Zhijun Liu, John L. Tan, Daniel M. Cohen et al., *Proc Natl Acad Sci U S A* 107 (22), 9944 (2010);**

Zenon Rajfur, Partha Roy, Carol Otey et al., *Nat Cell Biol* 4 (4), 286 (2002); Shigenobu Yonemura, Yuko Wada, Toshiyuki Watanabe et al., *Nat Cell Biol* 12 (6), 533 (2010).

[15]   A. J. Engler, P. O. Humbert, B. Wehrle-Haller et al., *Science* 324 (5924), 208 (2009).

[16]   Celeste M. Nelson, Ronald P. Jean, John L. Tan et al., *Proc Natl Acad Sci U S A* 102 (33), 11594 (2005); Celeste M. Nelson, Martijn M. VanDuijn, Jamie L. Inman et al., *Science* 314 (5797), 298 (2006).

[17]   Benjamin Geiger, Joachim P. Spatz, and Alexander D. Bershadsky, *Nat Rev Mol Cell Biol* 10 (1), 21 (2009).

[18]   Pere Roca-Cusachs, Nils C. Gauthier, Armando del Rio et al., *Proc Natl Acad Sci U S A* 106 (38), 16245 (2009).

[19]   R. Krishnan, C. Y. Park, Y. C. Lin et al., *PLoS ONE* 4 (5), e5486 (2009); X Trepat, L Deng, SS An et al., *Nature* 447, 592 (2007).